

Attention, please: A Spatio-temporal Transformer for 3D Human Motion Prediction

Emre Aksan^{*1}, Peng Cao^{*1,2}, Manuel Kaufmann¹, and Otmar Hilliges¹

¹ ETH Zurich, Department of Computer Science

² Peking University, School of Electronics Engineering and Computer Science
 {emre.aksan, manuel.kaufmann, otmar.hilliges}@inf.ethz.ch
 caopeng2016@pku.edu.cn

Abstract. In this paper, we propose a novel architecture for the task of 3D human motion modelling. We argue that the problem can be interpreted as a generative modelling task: A network learns the conditional synthesis of human poses where the model is conditioned on a seed sequence. Our focus lies on the generation of plausible future developments over longer time horizons, whereas previous work considered shorter time frames of up to 1 second. To mitigate the issue of convergence to a static pose, we propose a novel architecture that leverages the recently proposed self-attention concept. The task of 3D motion prediction is inherently spatio-temporal and thus the proposed model learns high dimensional joint embeddings followed by a decoupled *temporal* and *spatial* self-attention mechanism. The two attention blocks operate in parallel to aggregate the most informative components of the sequence to update the joint representation. This allows the model to access past information directly and to capture spatio-temporal dependencies explicitly. We show empirically that this reduces error accumulation over time and allows for the generation of perceptually plausible motion sequences over long time horizons as well as accurate short-term predictions. Accompanying video available at <https://youtu.be/yF0cdt2yCNE>.

Keywords: 3D Motion Modelling, Spatio-temporal Models, Self-attention, Transformer

1 Introduction

Imagine a person running or riding a bicycle – while your inner depiction of human motion may not be an accurate prediction of an actual motion sequence, we are able to effortlessly forecast the complex dynamics of human motion in a plausible fashion over arbitrarily long time horizons. Despite much recent progress on 3D human motion modeling, this task remains challenging for machines, particularly when predicting motion over long time frames. In this context it is noteworthy

^{*}The first two authors contributed equally to this work. Peng performed this work during an internship at ETH.

that most previous works define short-term prediction as 0.5 seconds and long-term prediction as 1 second, respectively. In this paper we ask the question if machines can learn to predict plausible human motion over longer time frames in the order of magnitude of 5-20 seconds. Having access to such a model would have significant implications for many application domains, including self-driving cars, robotics and human computer interaction.

From a learning perspective the problem of 3D human motion modeling can be seen as a generative modeling task: A network learns conditional synthesis of sequences of human poses where the model is conditioned on the seed sequence. Hence, we hypothesize that a model that is truly capable of learning motion dynamics should be able to generate natural motion sequences over arbitrarily long horizons. In particular, such a model should not be limited to very short time horizons, especially for periodic motion types such as walking and running. However, most existing work typically suffers from a collapse to a static pose, suggesting a lack of ability to accurately capture long-term motion dependencies.

Given the temporal nature of human motion, it is not surprising that recurrent neural networks (RNNs) are the most popular architectural choice for the task [2, 10, 18, 24, 27, 32]. RNNs model the short and long-term dependencies by propagating information through their hidden state. Convolutional neural networks (CNN) in a sequence-to-sequence framework have also been proposed for this task [20], sometimes combined with spatial priors [21]. Such models follow an auto-regressive approach, factorizing the predictions into step-wise conditionals based on the previous predictions. This auto-regressive approach causes the model to accumulate error over time and eventually the predictions collapse to a non-plausible *static pose*. This issue is often associated with the exposure bias problem [28] due to the discrepancy between real and predicted distributions. To mitigate this problem, previous works use model predictions during training [24, 27] or apply noise on the model inputs [2, 18, 20]. Ghosh *et al.* [11] propose a de-noising autoencoder to reduce prediction drift. Since the task becomes harder as the distance between relevant steps increases, it has been proposed to leverage adversarial losses [20, 32] to better match the real distribution.

In this work, we present a novel architecture for the 3D human motion modeling task, which considers the spatio-temporal aspects of the data explicitly without relying on the propagation of a hidden state. Our approach is motivated by the recent success of the Transformer model [30] on many tasks such as modeling natural language [8, 30], music [16] and images [6, 26]. While the vanilla Transformer is designed for 1D sequences with a self-attention mechanism [3, 25, 30], we note that the task of 3D motion prediction is inherently spatio-temporal and we propose to decouple the temporal and spatial dimensions.

To do so, we project every joint onto a higher dimensional representation space that learns *joint embeddings*. For every joint we define *temporal attention* over the same joint in the past and *spatial attention* over the other joints at the same time step (see Fig. 1). The two attention blocks operate in parallel to identify the most informative components and aggregate this information to update the

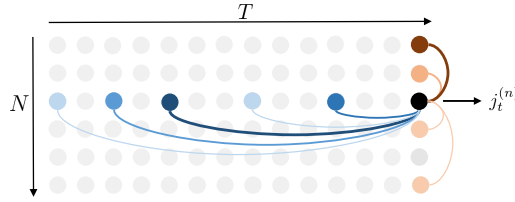


Fig. 1: **Illustration of the decoupled 2D attention.** The motion sequence is represented as a matrix where each cell represents the configuration of a single joint n at a specific time instance t . Height N and width T of the matrix correspond to the number of joints and time steps, respectively. For a particular joint (illustrated in black), the *temporal attention* considers all the past instances of the same joint (in blue) whereas the *spatial attention* is applied on the other joints in the skeleton (in red). The color shading illustrates the attention weights.

joint representation. To predict future steps, the sequence is summarized as a weighted combination of the representations in the previous steps. This dual self-attention over the sequence allows the model to access past information directly and hence capture the dependencies explicitly [25, 30], mitigating the error accumulation over time. This design furthermore introduces interpretability since the attention weights indicate the most informative sequence components that led to the prediction.

Following the protocol introduced by [2], we thoroughly evaluate our proposed model on the H3.6M [17] and AMASS [22] datasets both in the short- and long-term prediction setting. In our paper, AMASS serves as the primary test bed for long term predictions due to its richer corpus of motion sequences. We show experimentally that the spatio-temporal self-attention concept alleviates the collapse to static poses, particularly in long-term predictions and also that it is helpful for short-term predictions compared to its vanilla counterpart and other SoA models. We qualitatively show that our model is able to produce high-quality long-term predictions (up to 20 seconds for periodic motions such as walking and running). Although quantitative analysis becomes more challenging over such long horizons, we provide a distribution-based analysis showing that the self-attention concept shows strong performance in learning motion dynamics. Furthermore, we visualize the spatio-temporal dependencies captured by the model, providing insights into how the model forms its predictions.

2 Related Work

Recurrent Models RNNs have been the most popular architecture for 3D motion modeling tasks [2, 7, 9–11, 18, 31]. Fragkiadaki *et al.* [10] propose the Encoder-Recurrent-Decoder (ERD) model where input poses are encoded into a latent space before feeding them into an LSTM cell and decoding them to the output space. Jain *et al.* [18] build a skeleton like st-graph with RNNs as nodes. Aksan *et al.* [2] replace the dense output layer of a RNN architecture

with a structured prediction layer that follows the kinematic chain. The authors furthermore introduce a large-scale human motion dataset, AMASS [22], to the task of motion prediction. In such approaches the error accumulation problem is typically mitigated to a limited extent by exposing the model to dropout or Gaussian noise during training. Ghosh *et al.* [11] more explicitly train a separate de-noising autoencoder that refines the noisy RNN predictions.

Martinez *et al.* [24] introduce a sequence-to-sequence (seq2seq) architecture and skip connection from input to output on the decoder to address the transition problems between the seed and predicted poses. They also propose training the model with the predictions to alleviate the exposure bias problem. Similarly, Pavlo *et al.* [27] suggest using a teacher-forcing ratio to gradually expose the model to its own predictions during training. In [7], the seq2seq framework is modified to explicitly model different time scales using a hierarchy of RNNs. Gui *et al.* [32] propose a geodesic loss and adversarial training and Wang *et al.* [31] replace the likelihood objective with imitation via policy gradient methods.

While the use of domain-specific priors and objectives can improve short term accuracy, the inherent problems of the underlying RNN architectures still exist. Maintaining long-term dependencies is an issue due to the need of summarizing the entire history in a hidden state of fixed-size. Inspired by similar observations in the field of NLP [25,30], we introduce a spatio-temporal self-attention mechanism to mitigate this problem. In doing so we let the network explicitly reason about past frames without the need to compress the past into a single hidden vector.

Non-recurrent Models Bütetage *et al.* [4,5] use dense layers on sliding windows from the motion sequences. In [14,15] convolutional models are introduced for motion synthesis conditioned on trajectories. More recently, Hernandez *et al.* [13] propose to treat motion prediction as an image inpainting task and use a convolutional model with adversarial losses. Joints are represented as positions in 3D space, often requiring auxiliary losses such as bone length and joint limits to ensure anatomical consistency. Li *et al.* [20] use CNNs instead of RNNs in the sequence-to-sequence framework to alleviate the issues of learning long-term dependencies. The authors propose decoupling the short- and long-term context by using dedicated networks and train the model with an adversarial loss.

Mao *et al.* [23] represent sequences of joints via discrete cosine transform (DCT) coefficients. Furthermore, they train a graph convolutional network (GCN) on the human skeleton to learn inter-joint dependencies, achieving state-of-the-art performance on H3.6M. Our proposed spatial attention is functionally similar to the GCN in the sense that both networks learn to identify informative joints in the skeleton. While the GCN operates on a short window of poses represented by DCT coefficients, our spatial attention block considers a single frame. Hence, we claim that our 2D-transformer architecture can be scaled to arbitrarily long sequences. It is technically possible to deploy the GCN in a sliding window-fashion to make long-term predictions, but this is not demonstrated or mentioned in [23].

In summary, we propose a novel 2D transformer architecture that is capable of making accurate short-term and plausible long-term predictions up to 20 seconds. Most existing works have introduced regularization techniques, auxiliary

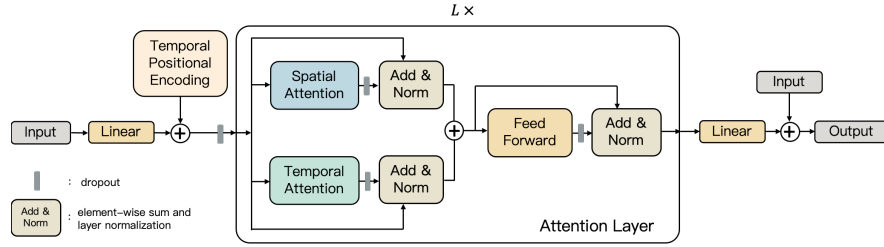


Fig. 2: **Architecture overview.** We start by projecting every joint into an embedding space. After injecting positional encodings and applying dropout, the embeddings are then fed to L consecutive attention layers. We employ a novel spatio-temporal multi-head attention mechanism based on [30]. It is split into a *temporal* attention block that updates a joint’s embedding by looking at the past instances of the same joint and a *spatial* block that attends over all the joints in the current time step. Finally, we estimate the next pose by projecting the embeddings back to the joint space and using a residual connection from input to output, following [24].

loss terms or adversarial objectives to circumvent the inherent problems of the underlying architectures, making these models often hard to train. We show that the self-attention concept is very effective in learning motion dynamics and allows for the design of a versatile mechanism that is simple, effective and easy to train.

3 Method

This section explains the proposed 2D-transformer architecture. For an overview please refer to Fig. 2.

Our approach first decomposes the skeleton into joints and independently projects them onto a higher dimensional representation space. This step can be considered as learning embeddings for joint angles. We later refine the joint representation by using the relevant inter- and intra-joint dependencies which are identified by the attention blocks. Finally, we assemble the skeleton from the predicted joints which constitutes the next pose. Our method uses the building blocks of the Transformer [30], but with two main differences: (1) a decoupled spatio-temporal attention mechanism and (2) a fully auto-regressive model.

To capture the inherent spatio-temporal aspect of human motion, we design a novel 2D attention mechanism. This mechanism is trained to identify useful information from the known sequence to construct the next output pose. The spatial attention block draws information from the joint features at the current time step whereas the temporal block focuses on distilling information from the previous records of individual joints. This scheme not only reveals the dependencies between joints and frames but also provides insights into how the model forms predictions. Our model does not follow the sequence-to-sequence paradigm as we do not consider the seed sequence only as a conditioning context. Instead, our model is trained to predict the next step given the past steps similar to RNNs. In other words, the temporal attention block operates on variable-length

sequences. Note that our model is auto-regressive, predicting the next pose given the past predictions.

3.1 Problem Formulation

A motion sample can be represented by a sequence $\mathbf{X} = \{\mathbf{x}_1, \dots, \mathbf{x}_T\}$ where a frame $\mathbf{x}_t = \{\mathbf{j}_t^{(1)}, \dots, \mathbf{j}_t^{(N)}\}$ denotes a pose at time step t with joints $\mathbf{j}_t^{(n)} \in \mathbb{R}^M$. Each joint \mathbf{j} is an M -dimensional vector where M is determined by the pose parameterization, e.g., 3D position, rotation matrix, angle-axis or quaternion. In this work we use a rotation matrix representation, i.e., $M = 9$.

Following a predefined order, a sequence sample \mathbf{X} can be written as a matrix of size $NM \times T$:

$$\mathbf{X} = \begin{bmatrix} \mathbf{j}_1^{(1)} & \mathbf{j}_2^{(1)} & \dots & \mathbf{j}_T^{(1)} \\ \mathbf{j}_1^{(2)} & \mathbf{j}_2^{(2)} & \dots & \mathbf{j}_T^{(2)} \\ \vdots & \vdots & \ddots & \vdots \\ \mathbf{j}_1^{(N)} & \mathbf{j}_2^{(N)} & \dots & \mathbf{j}_T^{(N)} \end{bmatrix} \quad (1)$$

where each block of M consecutive rows represents a single joint and a column corresponds to a full pose.

In our notation the subscript denotes the time step. We use n -tuples in the superscript ordered by joint index, layer index, and optionally attention head index. For example, $\mathbf{W}^{(n,I)}$ stands for the weight matrix of the input (I) of joint n . Please note that projection matrices \mathbf{W} and bias terms \mathbf{b} are trainable. n in the superscript indicates that it is only used by joint n .

3.2 Spatio-temporal Transformer

Joint Embeddings We first project all joints into a D -dimensional space via a single linear layer:

$$\mathbf{e}_t^{(n)} = \mathbf{W}^{(n,E)} \mathbf{j}_t^{(n)} + \mathbf{b}^{(n,E)} \quad (2)$$

where $\mathbf{W}^{(n,E)} \in \mathbb{R}^{D \times M}$ and $\mathbf{b}^{(n,E)} \in \mathbb{R}^D$ correspond to the weight and bias in the embedding layer for joint n , respectively. In our experiments we set $D = 128$ and $D = 64$ for AMASS and H3.6M datasets, respectively.

Unlike RNNs or CNNs, the Transformer has no notion of ordering within a sequence. Following [30], we inject sinusoidal positional encoding into the joint embeddings, reported to be helpful in extrapolating to longer sequences [30].

After applying dropout [29], the joint embeddings are passed to a stack of L attention blocks where we apply temporal and spatial attention in parallel and update the embeddings.

Temporal Attention In the temporal attention block, the embedding of every joint is updated by using the past frames of the same joint. Formally, for each joint $n \in \{1, \dots, N\}$, we calculate a temporal summary $\bar{\mathbf{E}}^{(n)} = [\bar{\mathbf{e}}_1^{(n)}, \dots, \bar{\mathbf{e}}_T^{(n)}]^T \in \mathbb{R}^{T \times D}$.

We use the scaled dot-product attention proposed by [30], requiring *query*, \mathbf{Q} , *key*, \mathbf{K} , and *value* \mathbf{V} representations. Intuitively, the *value* corresponds to the set of past representations that are indexed by the *keys*. For the joint of interest, we compare its *query* representation with all *keys* w.r.t. the dot-product similarity. If the *query* and the *key* are similar (i.e., high attention weight), then it means that the corresponding *value* is relevant. The result of the attention operation is the weighted sum of the *values* \mathbf{V} :

$$\text{Attention}(\mathbf{Q}, \mathbf{K}, \mathbf{V}, \mathbf{M}) = \text{softmax} \left(\frac{\mathbf{Q}\mathbf{K}^T}{\sqrt{D}} + \mathbf{M} \right) \mathbf{V} = \mathbf{A}\mathbf{V}, \quad (3)$$

where the mask \mathbf{M} prevents information leaking from future steps. For the temporal attention mechanism, we refer to matrix \mathbf{A} as $\bar{\mathbf{A}} \in \mathbb{R}^{T \times T}$. It contains the temporal attention weights, where each row i in $\bar{\mathbf{A}}$ represents how much attention is paid to the previous frames in the sequence.

The \mathbf{Q}, \mathbf{K} and \mathbf{V} matrices are projections of the input embeddings $\mathbf{E}^{(n)} = [\mathbf{e}_1^{(n)}, \dots, \mathbf{e}_T^{(n)}]^T \in \mathbb{R}^{T \times D}$. Following [30], we use a multi-head attention (MHA) mechanism to project the D -dimensional representation into subspaces calculated by different attention heads $i \in \{1, \dots, H\}$:

$$\begin{aligned} \mathbf{Q}^{(n,i)} &= \mathbf{E}^{(n)} \mathbf{W}^{(n,Q,i)}, \quad \mathbf{Q}^{(n,i)} \in \mathbb{R}^{T \times F} \\ \mathbf{K}^{(n,i)} &= \mathbf{E}^{(n)} \mathbf{W}^{(n,K,i)}, \quad \mathbf{K}^{(n,i)} \in \mathbb{R}^{T \times F} \\ \mathbf{V}^{(n,i)} &= \mathbf{E}^{(n)} \mathbf{W}^{(n,V,i)}, \quad \mathbf{V}^{(n,i)} \in \mathbb{R}^{T \times F} \end{aligned} \quad (4)$$

where we set $F = D/H$. We use $H = 8$ and $H = 4$ attention heads in our model for AMASS and H3.6M datasets, respectively. Using multiple heads allows the model to gather information from different sets of timesteps into a single embedding. For example, every head in a MHA with 4 heads, outputs 16D chunks of a 64D representation. Hence, different attention heads enable accessing different components. The results are then concatenated and projected back into representation space using the weight matrix $\mathbf{W}^{(n,O)} \in \mathbb{R}^{HF \times D}$

$$\begin{aligned} \text{head}_i &= \text{Attention} \left(\mathbf{Q}^{(n,i)}, \mathbf{K}^{(n,i)}, \mathbf{V}^{(n,i)}, \mathbf{M} \right) \\ \bar{\mathbf{E}}^{(n)} &= \text{Concat}(\text{head}_1, \dots, \text{head}_H) \mathbf{W}^{(n,O)}. \end{aligned} \quad (5)$$

Spatial Attention In the vanilla Transformer, the attention block operates on the entire input vector \mathbf{x}_t where the relation between the elements are implicitly captured. We introduce an additional spatial attention block to learn inter-joint dependencies from the data explicitly. This allows the model to learn dynamic joint dependencies.

In contrast to the temporal counterpart, it attends over all joints of the same timestep. Moreover, the projections we use to calculate the *key* and *value* are shared across joints. Since we aim to identify the most relevant joints, we project them into the same embedding space and compare with the joint of interest.

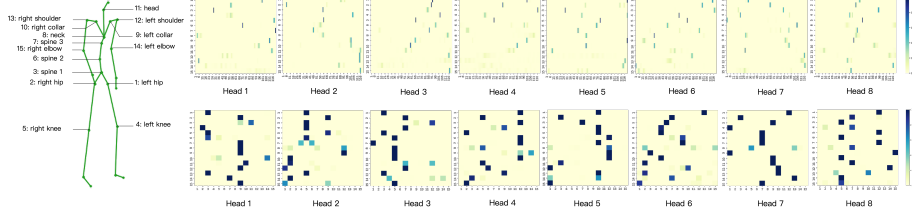


Fig. 3: Temporal (*top*) and spatial (*bottom*) attention weights of the first layer given 120 frames. Each row corresponds to a joint’s attention pattern. The columns stand for time-steps and joints for the temporal and spatial attention matrices, respectively. We visualize 8 heads showing that they attend to different joints and timesteps. Similarly, the relevant joints and timesteps differ with respect to the joint of interest.

For a given pose embedding $\mathbf{E}_t = [\mathbf{e}_t^{(1)}, \dots, \mathbf{e}_t^{(N)}]^T \in \mathbb{R}^{N \times D}$, the spatial summary of joints $\tilde{\mathbf{E}}_t^{(n)}$ is calculated as a function of all other joints by using the multi-head attention:

$$\begin{aligned}
 \mathbf{Q}_t^{(i)} &= \left[\left(\mathbf{W}^{(1,Q,i)} \right)^T \mathbf{e}_t^{(1)}, \dots, \left(\mathbf{W}^{(N,Q,i)} \right)^T \mathbf{e}_t^{(N)} \right]^T \\
 \mathbf{K}_t^{(i)} &= \mathbf{E}_t \mathbf{W}^{(K,i)} \\
 \mathbf{V}_t^{(i)} &= \mathbf{E}_t \mathbf{W}^{(V,i)} \\
 \text{head}_i &= \text{Attention}(\mathbf{Q}_t^{(i)}, \mathbf{K}_t^{(i)}, \mathbf{V}_t^{(i)}, \mathbf{0}) = \tilde{\mathbf{A}} \mathbf{V}_t^{(i)} \\
 \tilde{\mathbf{E}}_t^{(n)} &= \text{Concat}(\text{head}_1, \dots, \text{head}_H) \mathbf{W}^{(O)}
 \end{aligned} \tag{6}$$

where $\mathbf{Q}_t^{(i)} \in \mathbb{R}^{N \times S}$, $\mathbf{K}_t^{(i)} \in \mathbb{R}^{N \times S}$, $\mathbf{V}_t^{(i)} \in \mathbb{R}^{N \times S}$, $S = F = D/H$, $\text{head}_i \in \mathbb{R}^{N \times S}$, and $\mathbf{W}^{(O)} \in \mathbb{R}^{HS \times D}$. The spatial attention matrix $\tilde{\mathbf{A}} \in \mathbb{R}^{N \times N}$ represents how much attention each joint i pays to every other joint j including itself. Since it iterates over the joints in the same time-step, we no longer require a mask.

Aggregation The temporal and spatial attention blocks run in parallel to calculate summaries $\bar{\mathbf{E}}$ and $\tilde{\mathbf{E}}$, respectively. They are summed and passed to a 2-layer pointwise feedforward network [30], which is followed by dropout and layer normalization. We stack L such attention layers to successively update the joint embeddings. In other words, the output of an attention layer is input to the next one. Hence, stacking several attention layers helps refining the joint embeddings to predict the next pose.

Joint Predictions Finally, the joint prediction $\hat{\mathbf{j}}_{t+1}^{(n)}$ is obtained by projecting the corresponding D -dimensional joint embedding $\mathbf{e}_t^{(n)}$ from the L -th attention layer back into the M -dimensional joint angle space. Following [24], we apply a residual connection between the previous pose and our predictions.

Table 1: **H3.6M results** for *walking*, *eating*, *smoking* and *discussion* activities. Values are the Euler angle metric measured at the given time step (lower is better). ST-Transformer stands for our Spatio-temporal Transformer model, consistently outperforming the vanilla Transformer. DCT-GCN (ST) [23] stands for the short-term model which is designed to make predictions up to 400 ms. DCT-GCN (LT) has a 1 sec prediction horizon while the remaining models can make arbitrarily long predictions auto-regressively.

	Walking				Eating				Smoking				Discussion			
milliseconds	80	160	320	400	80	160	320	400	80	160	320	400	80	160	320	400
Zero-Velocity [24]	0.39	0.68	0.99	1.15	0.27	0.48	0.73	0.86	0.26	0.48	0.97	0.95	0.31	0.67	0.94	1.04
Seq2seq. [24]	0.28	0.49	0.72	0.81	0.23	0.39	0.62	0.76	0.33	0.61	1.05	1.15	0.31	0.68	1.01	1.09
AGED [32]	0.22	0.36	0.55	0.67	0.17	0.28	0.51	0.64	0.27	0.43	0.82	0.84	0.27	0.56	0.76	0.83
DCT-GCN (ST) [23]	0.18	0.31	0.49	0.56	0.16	0.29	0.50	0.62	0.22	0.41	0.86	0.80	0.20	0.51	0.77	0.85
DCT-GCN (LT) [23]	0.20	0.34	0.52	0.59	0.17	0.31	0.52	0.64	0.23	0.42	0.85	0.80	0.22	0.58	0.87	0.96
Transformer	0.25	0.42	0.67	0.79	0.21	0.32	0.54	0.68	0.26	0.49	0.94	0.90	0.31	0.67	0.95	1.04
ST-Transformer	0.21	0.36	0.58	0.63	0.17	0.30	0.49	0.60	0.22	0.43	0.88	0.82	0.19	0.52	0.79	0.88

3.3 Training and Inference

We train our model by predicting the next step both for the seed and the target sequences. We use the per-joint ℓ_2 distance on rotation matrices [2]:

$$\mathcal{L}(\mathbf{X}, \hat{\mathbf{X}}) = \sum_{t=2}^{T+1} \sum_{n=1}^N \left\| \mathbf{j}_t^{(n)} - \hat{\mathbf{j}}_t^{(n)} \right\|_2$$

At test time, we compute the prediction in an auto-regressive manner. That is, given a pose sequence $\{\mathbf{x}_1, \dots, \mathbf{x}_T\}$, we get the prediction $\hat{\mathbf{x}}_{T+1}$. Due to memory limitations, we apply the temporal attention over a sliding window of poses which we set as the length of the seed sequence. In other words, to produce $\hat{\mathbf{x}}_{T+2}$ we condition on the sequence $\{\mathbf{x}_2, \dots, \hat{\mathbf{x}}_{T+1}\}$.

4 Experiments

We compare our model with the state-of-the-art methods quantitatively in Sec. 4.1 and qualitatively in Sec. 4.2. In Sec. 4.3, we provide insights into the dynamics of our spatio-temporal transformer model by visualizing the attention weights. Finally, we validate design choices through ablation studies in Sec. 4.4.

Datasets and Metrics We evaluate our model on the AMASS [22] and H3.6M [17] datasets, following the evaluation protocols of [2, 24], respectively. The AMASS benchmark provides a larger and more diverse set of motions compared to H3.6M. The frame rates also differ between AMASS and H3.6M, namely 60 and 25, introducing a significant difference in the 2 sec seed sequence length.

In addition to the standard metrics in [2, 24], we conduct further analysis by using complementary metrics in the frequency domain. Gopalakrishnan *et al.* [12] propose the normalized power spectrum similarity (NPSS) metric to evaluate predictions in the frequency domain. In contrast to the mean-squared loss, NPSS tolerates artifacts like shifted or skipped frames by comparing the

Table 2: **Analysis on the H3.6M** with different metrics in the short- (400 ms) and long-term (1 sec) setting (lower is better). We present the average of the four main actions (i.e., *walking*, *eating*, *smoking* and *discussion*) and all 15 actions in the dataset. DCT-GCN (ST) makes predictions only up to 400 ms. The *Euler* metric is the standard evaluation protocol in Table 1. *PS KLD* [13] stands for the symmetric KL-divergence between the prediction and test distributions in the frequency domain. *NPSS* [12] stands for normalized power spectrum similarity, comparing the ground-truth and predicted samples in the frequency domain. In both *PS KLD* and *NPSS*, predictions that have similar statistics to the ground-truths are still rewarded albeit not being identical. Note that our model’s performance is comparable to the DCT-GCT models.

metrics	Main (400 ms)		All (400 ms)		Main (1000 ms)			All (1000 ms)		
	Euler	PS KLD	Euler	PS KLD	Euler	PS KLD	NPSS	Euler	PS KLD	NPSS
VGRU-r1 [12]	0.99	n/a	n/a	n/a	1.69	n/a	0.130	n/a	n/a	n/a
DCT-GCN (ST) [23]	0.71	0.018	0.95	0.048	-	-	-	-	-	-
DCT-GCN (LT) [23]	0.75	0.020	0.97	0.052	1.26	0.065	0.074	1.590	0.096	0.126
ST-Transformer	0.73	0.015	1.02	0.040	1.31	0.072	0.073	1.722	0.091	0.131

frequency coefficients of the ground-truth and predicted motion samples. Similarly, Ruiz *et al.* [13] propose a distribution-based metric in the power spectrum (PS) space. Instead of a pairwise comparison, it measures the discrepancy between the prediction and test distributions by using KL-divergence (PS KLD). Inspired by the generative modelling literature, these metrics compare the statistics of the real and predicted motion data in the frequency domain.

Experiment details and our evaluation protocols are provided in the Appendix and the code will be made publicly available.

4.1 Quantitative Evaluation

We compare our approach with the SoA on the established H3.6M and the recent AMASS benchmarks. Following the previous work, we provide error metrics until 400-ms in detail. We also present quantitative longer-term analysis by using distribution-based metrics. Evaluations up to 1 sec are provided in the Appendix.

H3.6M Table 1 summarizes the results on the H3.6M dataset. Our Spatio-temporal Transformer outperforms the vanilla Transformer model, showing the benefits of our decoupled attention approach for motion modelling. AGED [32], the recently proposed cosine transformation based technique (dubbed DCT-GCN) [23] and our model share the state-of-the-art entries. The DCT-GCN method particularly excels in the *walking* category. We would like to note that DCT-GCN is trained with a pre-determined prediction horizon as it is designed to predict the entire 400 ms (i.e., ST) or 1 sec (i.e., LT) in one go. In contrast, Seq2seq, AGED and our model follow an auto-regressive approach. In other words, we can make arbitrarily long predictions at test time while DCT-GCN is limited to a particular horizon.

In Table 2, we further compare our model with DCT-GCN both in short- and long-term prediction horizons by using MSE and frequency domain metrics. We provide the VGRU-r1 model [12] as reference for the NPSS metric. We note that the STMI-GAN [13] results are not directly comparable because

Table 3: **AMASS results.** Lower is better for *Euler*, *Joint Angle* and *Positional* metrics. For the *Area Under the Curve (AUC)*, higher is better. ST-Transformer stands for our Spatio-temporal Transformer model. * indicates our own evaluation of the respective model. For more details how we evaluated [23] please refer to the appendix.

	Euler				Joint Angle				Positional				PCK (AUC)			
milliseconds	100	200	300	400	100	200	300	400	100	200	300	400	100	200	300	400
Zero-Velocity [2, 24]	1.91	5.93	11.36	17.78	0.37	1.22	2.44	3.94	0.14	0.48	0.96	1.54	0.86	0.83	0.84	0.82
Seq2seq [2, 24]	2.01	5.99	11.22	17.33	0.37	1.17	2.27	3.59	0.14	0.45	0.88	1.39	0.86	0.84	0.85	0.83
QuaterNet [2, 27]	1.49	4.70	9.16	14.54	0.26	0.89	1.83	3.00	0.10	0.34	0.71	1.18	0.90	0.87	0.88	0.85
RNN-SPL [2]	1.33	4.13	8.03	12.84	0.22	0.73	1.51	2.51	0.08	0.28	0.57	0.96	0.93	0.90	0.90	0.88
DCT-GCN (ST)* [23]	1.23	4.00	8.05	13.04	0.24	0.77	1.60	2.66	0.09	0.31	0.63	1.06	0.92	0.89	0.89	0.87
DCT-GCN (LT)* [23]	1.27	4.18	8.37	13.38	0.24	0.80	1.65	2.71	0.09	0.31	0.65	1.07	0.91	0.89	0.89	0.87
Transformer	1.30	4.01	7.88	12.69	0.22	0.73	1.52	2.54	0.08	0.28	0.58	0.97	0.92	0.90	0.90	0.88
ST-Transformer	1.11	3.61	7.31	12.04	0.20	0.68	1.45	2.48	0.08	0.27	0.57	0.97	0.93	0.90	0.90	0.88

STMI-GAN considers global translation and rotation predictions which all other models, including ours, do not. All metrics are calculated with the Euler angle representation by using the 15 main joints. Both NPSS and PS KLD metrics are computed over the corresponding sequence length (i.e., 400 ms and 1 sec). We observe that neither our ST-Transformer nor the DCT-GCN models can consistently outperform each other and that the comparable performance persists irrespective of the metric (cf. joint angle vs frequency domain).

The MSE metric on H36M is considered to be the de facto evaluation protocol in 3D motion prediction tasks. However, pairwise comparison rewards only the exact solution and penalizes slightly different but still plausible predictions. To alleviate this problem, Gopalakrishnan *et al.* [12] and Ruiz *et al.* [13] propose evaluation metrics in the frequency domain. It is also stated by Pavllo *et al.* [27] and Aksan *et al.* [2] that H3.6M evaluation exhibits high variance due to its limited size. Our detailed evaluation and inconclusive comparisons also implies that the H3.6M dataset is possibly saturated.

AMASS Table 3 summarizes the results with angle- and position metrics up to 400 ms. We compare our proposed Spatio-temporal Transformer model with the vanilla Transformer and previously reported RNN-based architectures. Our model achieves mostly better than state-of-the-art or similar performance in the short-term prediction task. Inline with the H3.6M results, our 2D decoupled attention mechanism is indeed beneficial when compared to the vanilla Transformer.

We would like to note that under our model the Euler metric improves the most. This can be explained by the similarity between our training objective and the metric. More specifically, the Euler metric calculates the error by using local joint angles after conversion into Euler angle representation, where our model is also trained to predict local angles, but directly in rotation matrix representation. Although the underlying joint angle representations are different, our joint-oriented architecture exploits the local information, leading to a better performance in a locality-based metric. Furthermore, our approach is fully generative and while it maintains local consistency, the global positions may deviate from the ground-truth under natural variation.

It is noteworthy to mention that the size of, and variety in motion types in AMASS are important to be able to learn motion dynamics accurately. In Figure 4, we compare our ST-Transformer model with the RNN-SPL baseline on AMASS for predictions up to 15 seconds, which is the longest prediction horizon presented so far in the literature. For such long horizons direct comparison to the seed

sequence via the MSE becomes increasingly problematic. To provide some quantitative analysis over long-term predictions we leverage the PS KLD metric (Fig. 4). The reference values (green) from the training and test samples are calculated on randomly extracted 1-second windows (i.e., 60 frames). Similarly, we compute statistics over the predictions (red and blue) by shifting a 1-second window. In other words, we compare every second of the prediction with real 1-second clips. As expected, the prediction statistics do deviate from the ground-truth statistics with increasing prediction horizon. However, our model remains much closer to the real data statistics than the RNN-SPL baseline - in particular so for long prediction horizons. Similarly the spatio-temporal transformer consistently yields better performance than the vanilla variant.

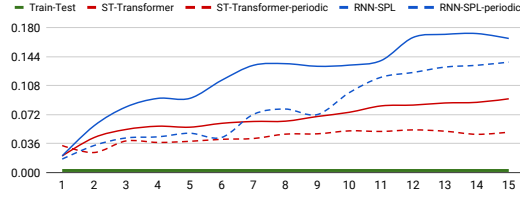


Fig. 4: Symmetric KLD of data and model distributions on Power Spectrum (PS KLD). Lower is better. Indication of the distance between training and prediction distributions. Our model (red) is closer to the training data for longer predictions. The RNN is worse even for periodic motions (dashed blue) due to convergence to the mean pose.

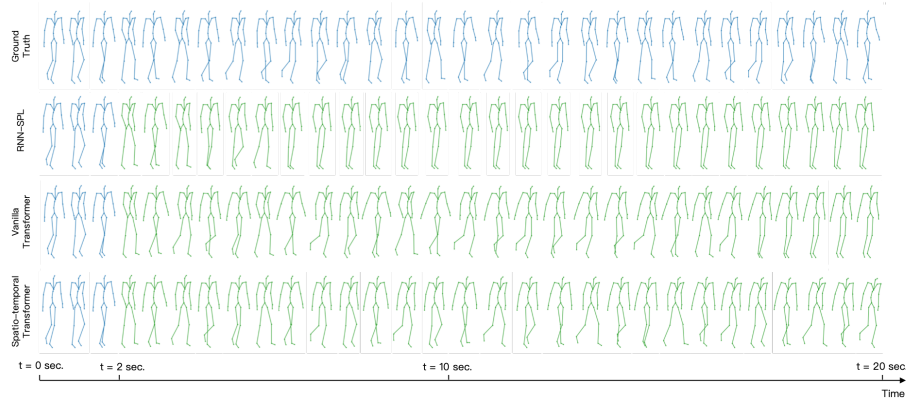


Fig. 5: A walking motion predicted by RNN-SPL [2], vanilla Transformer, and our Spatio-temporal Transformer. The length of the seed sequence is 2 seconds and the length of the whole sequence is 20 seconds.

4.2 Qualitative Evaluation

We evaluate the generative capabilities via conditional synthesis up to 20 seconds. In other words, we provide a particular motion sequence such as walking and predict autoregressively beyond its training horizon (i.e., 400 ms).

We qualitatively compare our model with the vanilla Transformer and RNN-SPL on a walking sample from the AMASS dataset (see Fig. 5). For RNN-SPL any variation quickly disappears within 5 seconds, indicating that it converges to a static pose. The vanilla Transformer mitigates this problem for longer and shows the benefits of the attention mechanism over recurrent networks. Finally, our proposed decoupled attention mechanism further improves and maintains the periodic patterns up to 20 seconds in this sample. We would like to note that the arms do not move as naturally as the ground-truth towards the end of the prediction, while the legs move naturally. More samples can be found in the appendix and video.

While our model performs well on periodic motions for long horizons, we acknowledge that the prediction horizon is limited to a few seconds for aperiodic motion types (which still exceeds previously reported horizons significantly). This is not unexpected since the model does not learn any transition patterns when trained on 2.4-second windows (i.e., 2 second seed and 400 ms target). Please also note that despite the quality of the results, the predictions deviate from the ground-truth, which makes sample-based metrics obsolete over longer horizons.

4.3 What does Attention Look Like?

The underlying attention mechanism of our model provides insights into the model’s predictions. In this section we visualize and discuss the attention patterns of our model on the AMASS dataset. In Fig. 3, we visualize the temporal and spatial attention weights $\bar{\mathbf{A}}$, $\hat{\mathbf{A}}$ that are used to predict the first frame given the seed sequence of 120 frames. In our visualizations, we used the first layer as it uses the initial joint embeddings directly. In the upper layers, the information is already gathered and hence the attention is dispersed.

First, we observe that there is a diverse set of attention patterns across heads, enriching the representation through gathering information from multiple sources. Second, the temporal attention weights reveal that the model is able to attend over a long horizon. While some heads focus on near frames, some look to the very beginning which would be difficult for an RNN. Finally, in the spatial attention, we observe joint-dependencies not only on the kinematic chain but also across the left and right parts of the skeleton. For example, while predicting the left knee joint, the model attends to the spine, left collar and right hip, knee and collar joints. Similarly, for the right elbow, the most informative joints are spine, the left collar, the hips and knee joints.

In order to adapt to changing spatio-temporal patterns, our model calculates the attention weights at every step. In Fig. 6, we visualize the change in the attention weights over time. The focus of the network changes as expected. Although the attention window shifts in time, we observe that for quasi-static

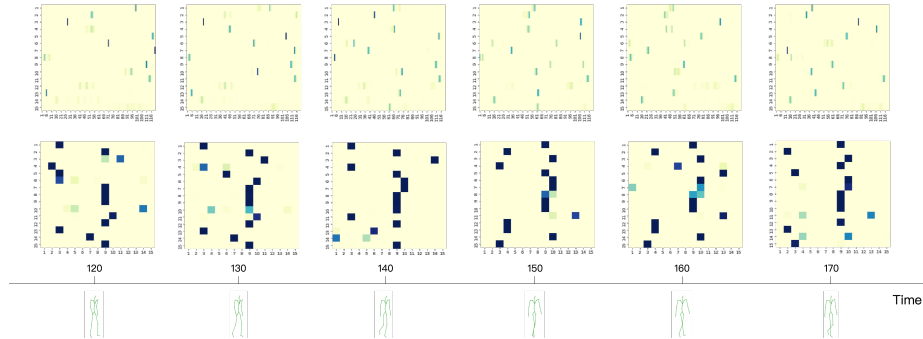


Fig. 6: Temporal (*top*) and spatial (*middle*) attention weights aligned with the poses (*bottom*) over 1 second prediction. We visualize a single head in the first layer. Our model identifies the informative joints dynamically. Note that the temporal attention is calculated over a sliding window. Some of the past frames remain in the focus of the temporal attention despite the shift in the inputs. Similarly, the spatial focus is preserved on the more static joints such as left and right collars (i.e., columns 9 and 10 in the middle row).

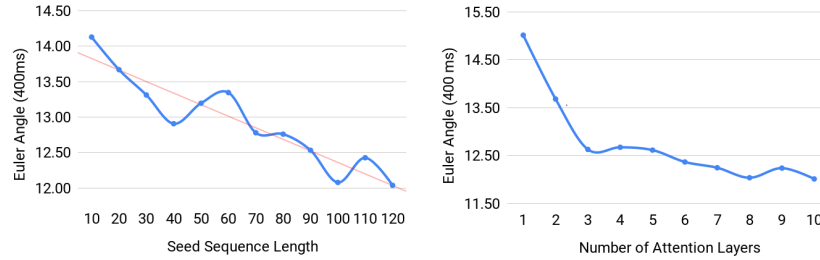


Fig. 7: Performance of our model when trained with seed sequence of different lengths (*left*) and different number of attention layers (*right*) on AMASS dataset.

joints like the hips or spine, the model maintains the focus on the same time-step in this particular attention head. When we calculate the inter-joint dependencies via spatial attention, a large number of joints attend to the left and right collars. This could indicate that such mostly static joints are used as reference.

4.4 Ablations

Figure 9 plots the performance of our model when trained with seed sequences of varying length, showing the performance w.r.t. the temporal attention window. The decreasing trend suggests that our model benefits from longer sequences. This hypothesis can also be supported via the temporal attention masks showing that our model accesses poses from the beginning of the sequence (cf. Fig. 3,6).

We train our model with varying number of layers. Fig. 9 shows that reasonable performance on AMASS is reached with only 3 layers. In our AMASS experiments, we use a model with 8 layers trained on a seed sequences of 120 steps whereas a 4-layer architecture with 50 input frames is used on the smaller H3.6M dataset.

5 Conclusion

We introduce a novel spatio-temporal transformer (ST-Transformer) network for the 3D human motion prediction task. We posit that the task can be interpreted as a pure generative modeling task and propose a novel architecture that learns intra- and inter-joint dependencies via its decoupled temporal and spatial attention blocks. We show that the self-attention concept is very effective in making both short- and long-term predictions. It mitigates the long-term dependency issue observed in RNN-based architectures and is able to synthesize motion sequences up to 20 seconds conditioned on periodic motion types such as walking or running. We also demonstrate that the attention mechanism can be used to attain insights about the model’s behavior. Finally, our ablation studies suggest that our model can make efficient use of large datasets with long seed sequences such as the recent AMASS.

References

1. Abadi, M., Agarwal, A., Barham, P., Brevdo, E., Chen, Z., Citro, C., Corrado, G.S., Davis, A., Dean, J., Devin, M., Ghemawat, S., Goodfellow, I., Harp, A., Irving, G., Isard, M., Jia, Y., Jozefowicz, R., Kaiser, L., Kudlur, M., Levenberg, J., Mané, D., Monga, R., Moore, S., Murray, D., Olah, C., Schuster, M., Shlens, J., Steiner, B., Sutskever, I., Talwar, K., Tucker, P., Vanhoucke, V., Vasudevan, V., Viégas, F., Vinyals, O., Warden, P., Wattenberg, M., Wicke, M., Yu, Y., Zheng, X.: TensorFlow: Large-scale machine learning on heterogeneous systems (2015), <https://www.tensorflow.org/>, software available from tensorflow.org
2. Aksan, E., Kaufmann, M., Hilliges, O.: Structured prediction helps 3d human motion modelling. In: The IEEE International Conference on Computer Vision (ICCV) (Oct 2019)
3. Al-Rfou, R., Choe, D., Constant, N., Guo, M., Jones, L.: Character-level language modeling with deeper self-attention. In: Proceedings of the AAAI Conference on Artificial Intelligence. vol. 33, pp. 3159–3166 (2019)
4. Bütepage, J., Black, M.J., Kragic, D., Kjellström, H.: Deep representation learning for human motion prediction and classification. 2017 IEEE Conference on Computer Vision and Pattern Recognition (CVPR) pp. 1591–1599 (2017)
5. Bütepage, J., Kjellström, H., Kragic, D.: Anticipating many futures: Online human motion prediction and generation for human-robot interaction. In: 2018 IEEE International Conference on Robotics and Automation, ICRA 2018, Brisbane, Australia, May 21–25, 2018. pp. 1–9 (2018). <https://doi.org/10.1109/ICRA.2018.8460651>, <https://doi.org/10.1109/ICRA.2018.8460651>
6. Child, R., Gray, S., Radford, A., Sutskever, I.: Generating long sequences with sparse transformers. arXiv preprint arXiv:1904.10509 (2019)
7. Chiu, H.K., Adeli, E., Wang, B., Huang, D.A., Niebles, J.C.: Action-agnostic human pose forecasting. 2019 IEEE Winter Conference on Applications of Computer Vision (WACV) pp. 1423–1432 (2018)
8. Devlin, J., Chang, M.W., Lee, K., Toutanova, K.: Bert: Pre-training of deep bidirectional transformers for language understanding. arXiv preprint arXiv:1810.04805 (2018)

9. Du, X., Vasudevan, R., Johnson-Roberson, M.: Bio-lstm: A biomechanically inspired recurrent neural network for 3d pedestrian pose and gait prediction. *IEEE Robotics and Automation Letters (RA-L)* (2019), accepted
10. Fragkiadaki, K., Levine, S., Felsen, P., Malik, J.: Recurrent network models for human dynamics. In: *Proceedings of the 2015 IEEE International Conference on Computer Vision (ICCV)*. pp. 4346–4354. ICCV '15, IEEE Computer Society, Washington, DC, USA (2015). <https://doi.org/10.1109/ICCV.2015.494>, <http://dx.doi.org/10.1109/ICCV.2015.494>
11. Ghosh, P., Song, J., Aksan, E., Hilliges, O.: Learning human motion models for long-term predictions. In: *2017 International Conference on 3D Vision, 3DV 2017, Qingdao, China, October 10-12, 2017*. pp. 458–466 (2017). <https://doi.org/10.1109/3DV.2017.00059>, <https://doi.org/10.1109/3DV.2017.00059>
12. Gopalakrishnan, A., Mali, A., Kifer, D., Giles, L., Ororbia, A.G.: A neural temporal model for human motion prediction. In: *Proceedings of the IEEE Conference on Computer Vision and Pattern Recognition*. pp. 12116–12125 (2019)
13. Hernandez, A., Gall, J., Moreno-Noguer, F.: Human motion prediction via spatio-temporal inpainting. In: *The IEEE International Conference on Computer Vision (ICCV)* (October 2019)
14. Holden, D., Saito, J., Komura, T.: A deep learning framework for character motion synthesis and editing. *ACM Trans. Graph.* **35**(4), 138:1–138:11 (Jul 2016). <https://doi.org/10.1145/2897824.2925975>, <http://doi.acm.org/10.1145/2897824.2925975>
15. Holden, D., Saito, J., Komura, T., Joyce, T.: Learning motion manifolds with convolutional autoencoders. In: *SIGGRAPH Asia 2015 Technical Briefs*. pp. 18:1–18:4. SA '15, ACM, New York, NY, USA (2015). <https://doi.org/10.1145/2820903.2820918>, <http://doi.acm.org/10.1145/2820903.2820918>
16. Huang, C.Z.A., Vaswani, A., Uszkoreit, J., Simon, I., Hawthorne, C., Shazeer, N., Dai, A.M., Hoffman, M.D., Dinculescu, M., Eck, D.: Music transformer: Generating music with long-term structure (2018)
17. Ionescu, C., Papava, D., Olaru, V., Sminchisescu, C.: Human3.6m: Large scale datasets and predictive methods for 3d human sensing in natural environments. *IEEE Transactions on Pattern Analysis and Machine Intelligence* **36**(7), 1325–1339 (jul 2014)
18. Jain, A., Zamir, A.R., Savarese, S., Saxena, A.: Structural-rnn: Deep learning on spatio-temporal graphs. In: *2016 IEEE Conference on Computer Vision and Pattern Recognition, CVPR 2016, Las Vegas, NV, USA, June 27-30, 2016*. pp. 5308–5317 (2016). <https://doi.org/10.1109/CVPR.2016.573>, <https://doi.org/10.1109/CVPR.2016.573>
19. Kingma, D.P., Ba, J.: Adam: A method for stochastic optimization. *arXiv preprint arXiv:1412.6980* (2014)
20. Li, C., Zhang, Z., Sun Lee, W., Hee Lee, G.: Convolutional sequence to sequence model for human dynamics. In: *The IEEE Conference on Computer Vision and Pattern Recognition (CVPR)* (June 2018)
21. Li, Y., Wang, Z., Yang, X., Wang, M., Poiana, S.I., Chaudhry, E., Zhang, J.: Efficient convolutional hierarchical autoencoder for human motion prediction. *The Visual Computer* **35**(6-8), 1143–1156 (2019)
22. Mahmood, N., Ghorbani, N., F. Troje, N., Pons-Moll, G., Black, M.J.: Amass: Archive of motion capture as surface shapes. In: *The IEEE International Conference on Computer Vision (ICCV)* (Oct 2019), <https://amass.is.tue.mpg.de>

23. Mao, W., Liu, M., Salzmann, M., Li, H.: Learning trajectory dependencies for human motion prediction. In: The IEEE International Conference on Computer Vision (ICCV) (October 2019)
24. Martinez, J., Black, M.J., Romero, J.: On human motion prediction using recurrent neural networks. In: Proceedings IEEE Conference on Computer Vision and Pattern Recognition (CVPR) 2017. IEEE, Piscataway, NJ, USA (Jul 2017)
25. Parikh, A.P., Täckström, O., Das, D., Uszkoreit, J.: A decomposable attention model for natural language inference. arXiv preprint arXiv:1606.01933 (2016)
26. Parmar, N., Vaswani, A., Uszkoreit, J., Kaiser, Ł., Shazeer, N., Ku, A., Tran, D.: Image transformer. arXiv preprint arXiv:1802.05751 (2018)
27. Pavlo, D., Grangier, D., Auli, M.: Quaternet: A quaternion-based recurrent model for human motion. In: British Machine Vision Conference 2018, BMVC 2018, Northumbria University, Newcastle, UK, September 3-6, 2018. p. 299 (2018), <http://bmvc2018.org/contents/papers/0675.pdf>
28. Ranzato, M., Chopra, S., Auli, M., Zaremba, W.: Sequence level training with recurrent neural networks. arXiv preprint arXiv:1511.06732 (2015)
29. Srivastava, N., Hinton, G., Krizhevsky, A., Sutskever, I., Salakhutdinov, R.: Dropout: a simple way to prevent neural networks from overfitting. *The journal of machine learning research* **15**(1), 1929–1958 (2014)
30. Vaswani, A., Shazeer, N., Parmar, N., Uszkoreit, J., Jones, L., Gomez, A.N., Kaiser, Ł., Polosukhin, I.: Attention is all you need. In: Guyon, I., Luxburg, U.V., Bengio, S., Wallach, H., Fergus, R., Vishwanathan, S., Garnett, R. (eds.) *Advances in Neural Information Processing Systems* 30, pp. 5998–6008. Curran Associates, Inc. (2017), <http://papers.nips.cc/paper/7181-attention-is-all-you-need.pdf>
31. Wang, B., Adeli, E., Chiu, H.k., Huang, D.A., Niebles, J.C.: Imitation learning for human pose prediction. In: The IEEE International Conference on Computer Vision (ICCV) (October 2019)
32. Wang, Y., Gui, L.Y., Liang, X., Moura, J.M.F.: Adversarial geometry-aware human motion prediction. In: European Conference on Computer Vision (ECCV). Springer (October 2018)

6 Appendix

In these supplementary materials, we provide additional details on the implementation of the proposed model and further experimental evidence of its performance. We explain the details of the metrics in the frequency domain and present further results on the AMASS dataset. We also report detailed results on the H3.6M dataset. Moreover we discuss the multi-head self-attention mechanism, which we use in both the temporal and the spatial attention blocks.

6.1 Experimental details

We implemented all models and run experiments using TensorFlow [1]. Hyper-parameters we used for the experiments are listed in Tab. 4. Due to the limited data size of H3.6M, we achieved better results by using a smaller network.

As suggested by Vasvani *et al.* [30], the Transformer architecture is sensitive to the learning rate. We apply the same learning rate schedule as proposed in [30]. The learning rate is calculated as a function of the training step as follows:

$$\text{learning rate} = D^{-0.5} \cdot \min(\text{step}^{-0.5}, \text{step} \times \text{warmup}^{-1.5}) \quad ,$$

where D is the joint embedding size. Warmup is set to 10000.

We use a batch size of 32 and the Adam optimizer [19] with its default parameters. Following the training protocol in [2], we apply early stopping with respect to the joint angle metric. Since our approach does not fall into the category of sequence-to-sequence (seq2seq) models, we use the entire sequence (i.e., seed and target) for training. On H3.6M, the temporal attention window size is set to 75 frames (i.e., 2-sec seed and 1-sec target at 25 fps). On AMASS, we fed the model with sequences of 120 frames (2-sec seed at 60 fps) due to memory limitations. We followed an auto-regressive approach and train our model by predicting the next pose given the frames so far. In other words, the input sequence is shifted by 1 step to attain the target frames.

Each attention block contains a feed forward network after the temporal and spatial attention layers. This feed forward network consists of two dense layers where the first one maps the $D = 128$ dimensional joint embeddings into

Table 4: Hyper-parameters for H3.6M and AMASS experiments.

	H3.6M	AMASS
Batch Size	32	32
Window size (num. frames)	75	120
Num. Attention Blocks (L)	4	8
Joint Embedding Size (D)	64	128
Num. Attention Heads (H)	4	8
Feedforward Size	128	256
Dropout Rate	0.1	0.1

256-dimensional space for AMASS (128-dimensional space for H3.6M), followed by a ReLU activation function. The second dense layer always projects back into the D -dimensional joint embedding space.

We use the same dropout rate of 0.1 for all dropout layers in our network.

6.2 Evaluation of DCT-GCN on AMASS

In Tab. 3 of the main paper we report the performance of the DCT-GCN model [23] on the AMASS dataset. The results correspond to the best results we obtained after hyper-parameter-tuning, explained in more detail in the following.

To train and evaluate the DCT-GCN on AMASS we used the code provided by Mao *et al.* but swapped out the data loading pipeline to load AMASS instead of H3.6M. As in the original paper, we train two networks - one for short-term (up to 400 milliseconds) and one for long-term (up to 1 second) predictions. In [23] the input to the network is 400 milliseconds (10 frames) worth of data. As AMASS is sampled at 60 Hz, we hence feed 24 frames as input and let the model predict 24 frames in the short-term case and 60 frames in the long-term case.

We fine-tuned the learning rate as well as the number of DCT coefficients. For the number of DCT coefficients we tried the original 35, but also the maximum number of coefficients (48 for short-term, 84 for long-term). As reported by [23] we found this to make little difference, but using 35 coefficients led to slightly better results.

The remaining hyper-parameters are as follows, which mostly follows the original setting. We are employing the Adam [19] optimizer with a learning rate of 0.001 and batch size of 16. We train for maximum 100 epochs with early stopping. The learning rate is decayed by a factor of 0.96 every other epoch. The input window size for the short-term model is 48 frames and 84 frames for the long-term model. The model parameters are kept as proposed in the original paper resulting in a model size of roughly 2.23 Mio. parameters.

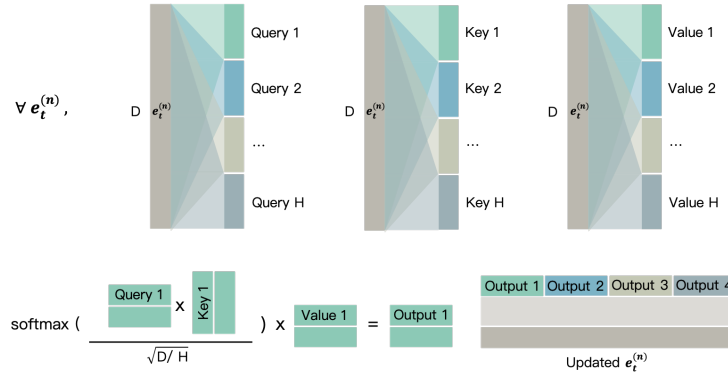


Fig. 8: The multi-head self-attention mechanism. Each color represents one head.

6.3 Multi-head Attention

Fig. 8 illustrates the multi-head self-attention mechanism. The sub-spaces of query, key and value for each attention head are calculated from the joint embeddings $\mathbf{e}_t^{(n)}$. From this figure it is clear that the joint embedding size D must be evenly divisible by the number of heads H . This in turn means the projection matrices involved for query, key, and value are of dimension $\mathbb{R}^{D \times \ell}$, where $\ell = D/H$. In the main paper we refer to ℓ as either S or F to distinguish between the temporal and spatial attention layer.

In the temporal attention blocks, we use separate query, key, and value weight matrices for different joints. In the spatial attention blocks, while the key and value weight matrices are shared across joints, the query weight matrices are not. Having obtained all the query, key, and value embeddings, we can get the output of each head according to Eq. (3) in the main submission. Note that the attention is over T time steps in the temporal attention blocks and N joints in the spatial attention blocks. Finally, the outputs from all of the heads are concatenated and then fed to the above mentioned feed forward network consisting of two dense layers and computing the updated embedding of $\mathbf{e}_t^{(n)}$.

6.4 Number of Attention Heads

In addition to the ablation experiments on the seed sequence length and number of attention layers, we train our model with a varying number of attention heads. As shown in Fig. 9, the best performance on AMASS is achieved with 8 attention heads. A model with 2 attention heads also yields reasonable performance. Comparison between the performance of multi- and single-head attention mechanism suggests that the model benefits from using more than one spatio-temporal configuration.

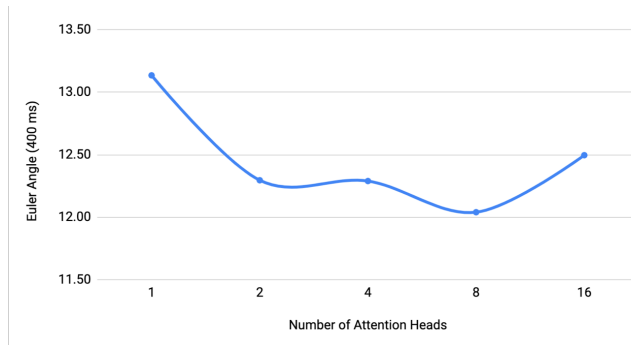


Fig. 9: Performance of our model when trained with different number of attention heads on AMASS dataset.

6.5 Power Spectrum Metrics on H3.6M dataset

We use the normalized power spectrum similarity (NPSS) [12] and power spectrum density KL-divergence (PS KLD) [13] metrics which have been proposed recently

as complementary measures to the commonly used MSE metric. Both NPSS and PS KLD metrics reward predictions exhibiting similar patterns with the ground-truths. Our evaluations focus on prediction horizons up to 400 ms and 1 sec on the H3.6M dataset as commonly reported in the literature.

Both metrics rely on motion statistics in the frequency domain. In our evaluations, we used the metrics “as-is” or with minimal modifications in order to adapt to our task and setting. We use publicly available implementations^{4 5}. Results are provided in Table 2 in the main submission.

Table 5: **PS Entropy results up to 15 seconds** (higher is better). We compare our model with RNN-SPL [2] on the entire test set and a subset of periodic motions, indicated by (P). We also provide the metric result on the real test distribution G as a reference. Lower values are an indication of the lack of activity. In other words, as the prediction horizon increases, models are likely to converge to the mean pose. We observe that RNN-based model significantly suffers from this problem as we hypothesize. In contrast, our model alleviates this issue thanks to our self-attention based concept.

seconds	1	2	3	4	5	6	7	8	9	10	11	12	13	14	15
Test	0.508	0.508	0.508	0.508	0.508	0.508	0.508	0.508	0.508	0.508	0.508	0.508	0.508	0.508	0.508
RNN-SPL	0.317	0.187	0.142	0.124	0.134	0.093	0.075	0.073	0.076	0.072	0.067	0.047	0.045	0.043	0.046
ST-Transformer	0.351	0.265	0.203	0.195	0.201	0.197	0.200	0.206	0.198	0.189	0.175	0.175	0.179	0.176	0.172
Test (P)	0.651	0.651	0.651	0.651	0.651	0.651	0.651	0.651	0.651	0.651	0.651	0.651	0.651	0.651	0.651
RNN-SPL (P)	0.519	0.320	0.300	0.322	0.327	0.298	0.193	0.180	0.193	0.151	0.094	0.083	0.077	0.076	0.065
ST-Transformer (P)	0.576	0.474	0.420	0.425	0.384	0.381	0.397	0.403	0.382	0.376	0.345	0.354	0.399	0.409	0.400

Table 6: **PS KLD results up to 15 seconds** (lower is better). We compare our model with RNN-SPL [2] on the entire test set and a subset of periodic motions, indicated by (P). We also provide the metric result between the real training and test distributions as the lower-bound. As the prediction horizon increases, prediction quality degrades, yet our model’s predictions remain closer to the real test distribution.

seconds	1	2	3	4	5	6	7	8	9	10	11	12	13	14	15
Train&Test	0.002	0.002	0.002	0.002	0.002	0.002	0.002	0.002	0.002	0.002	0.002	0.002	0.002	0.002	0.002
RNN-SPL	0.022	0.066	0.094	0.106	0.106	0.132	0.155	0.157	0.153	0.155	0.161	0.195	0.200	0.201	0.193
ST-Transformer	0.023	0.049	0.062	0.066	0.065	0.071	0.074	0.075	0.081	0.088	0.097	0.098	0.102	0.103	0.108
Train&Test (P)	0.015	0.015	0.015	0.015	0.015	0.015	0.015	0.015	0.015	0.015	0.015	0.015	0.015	0.015	0.015
RNN-SPL (P)	0.024	0.088	0.103	0.098	0.107	0.097	0.168	0.185	0.176	0.207	0.280	0.299	0.310	0.296	0.317
ST-Transformer (P)	0.020	0.032	0.061	0.069	0.073	0.084	0.084	0.090	0.102	0.117	0.122	0.120	0.122	0.111	0.115

NPSS We calculate the NPSS metric for both short- and long-term predictions (i.e., 400 ms and 1 sec) on the standard test samples in Euler angle representation. We consider only the active joints and discarded global translation and rotation entries as well. In other words, we use the same predictions and targets that are used to calculate the MSE metric in Table 1 in the main paper.

⁴ NPSS

⁵ PS KLD

PS KLD We use the same data as in the NPSS metric. As proposed in [13], we estimate power spectrum densities for the real and predicted sequences. We used the first 400-ms or 1-sec of the targets and predictions for the corresponding evaluation horizon. In contrast to [13], we do not use global translation and rotation. Moreover, our reported numbers correspond to the symmetric KL-divergence such that

$$PS\ KLD(G, P) = \frac{KLD(G||P) + KLD(P||G)}{2}, \quad (7)$$

where G and P are the power spectrum densities for the real and predicted samples, respectively. In our evaluation, we use the ground-truth targets as the real data. It is worthwhile to mention that PS KLD metric does not make pairwise comparisons. Instead, it measures the discrepancy between the real and predicted data distributions.

6.6 Power Spectrum Metrics on AMASS dataset

On AMASS dataset, we aim to show our model’s capability in making very long predictions (i.e., up to 15 – 20 sec). Note that such long prediction horizons prevents us from using pairwise metrics such as MSE or NPSS as the ground-truth targets are often much shorter than the prediction horizon. Hence, we use PS KLD and PS Entropy metrics proposed in [13].

In order to adapt the metrics into this new setup, we slightly modify the evaluation protocol we use on the H3.6M dataset. Instead of using the ground-truth targets, we randomly get 20000 sequences of length 1 sec (i.e., 60 frames) from the test dataset and calculate the power spectrum distribution G . Then, we get non-overlapping windows of 1 sec from the predictions to get $P_{t-1:t}$ where t stands for the corresponding prediction window. For example, $P_{5:6}$ is the power spectrum distribution for the predictions between 5 and 6 seconds. This enables us to measure the quality of arbitrarily long predictions by comparing every second of the predictions with the real reference data.

We use 3D positions instead of an angles as it is straightforward to convert any angle-based representation into positions by applying forward kinematics.

PS Entropy Convergence to the mean pose is a common issue with the RNN-based models. When there is a lack of activity, entropy naturally decreases. Table 5 compares our model with RNN-SPL [2] under the PS Entropy metric. We calculate the PS Entropy metric on every 1-sec prediction windows $P_{t-1:t}$ up to 15 seconds.

PS KLD In Table 6, we report symmetric PS KLD results. They are computed between G and $P_{t-1:t}$ where $t \in \{1, \dots, 15\}$ by using Eqn. 7.

Fig. 10 plots the data reported in Tables 5 and 6. Both evaluations with PS Entropy and PS KLD metrics indicate that our model alleviates the mean pose convergence problem and hence is capable of making very long predictions. For qualitative analysis, please refer to the supplementary video.

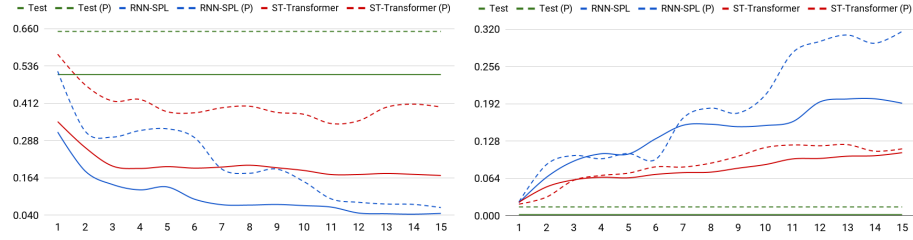


Fig. 10: **PS Entropy (left) and PS KLD (right) metrics.** Plots of the results reported in Tables 5 and 6. We would like to note that the PS KLD plot is slightly different from Fig. 4 in the main submission. Here we report the comparison between the predictions and the *test* data whereas in the paper we use *training* data statistics.

6.7 Detailed H3.6M Results

In Table 7 we provide short-term (i.e. up to 400 ms) evaluation results for all 15 actions. Similarly, Table 8, reports long-term (i.e., up to 1 sec) evaluations for 4 main actions which are reported by the baseline methods. Considering the evaluation results with MSE, NPSS and PS KLD metrics on H3.6M, our model is comparable to the baseline models and achieve SoA in specific cases. We would like to note that the comparable results achieved by a number of method implies that H3.6M benchmark is saturating for 3D motion prediction task.

Table 7: **Short-term H3.6M results** for all activities. Values are the Euler angle metric measured at the given time step (lower is better). ST-Transformer stands for our Spatio-temporal Transformer model. DCT-GCN (ST) [23] stands for the short-term model which is designed to make predictions up to 400 ms. DCT-GCN (LT) has a 1 sec prediction horizon while the remaining models can make arbitrarily long predictions auto-regressively.

milliseconds	Walking				Eating				Smoking				Discussion			
	80	160	320	400	80	160	320	400	80	160	320	400	80	160	320	400
Seq2seq. [24]	0.28	0.49	0.72	0.81	0.23	0.39	0.62	0.76	0.33	0.61	1.05	1.15	0.31	0.68	1.01	1.09
AGED [32]	0.22	0.36	0.55	0.67	0.17	0.28	0.51	0.64	0.27	0.43	0.82	0.84	0.27	0.56	0.76	0.83
DCT-GCN (ST) [23]	0.18	0.31	0.49	0.56	0.16	0.29	0.50	0.62	0.22	0.41	0.86	0.80	0.20	0.51	0.77	0.85
DCT-GCN (LT) [23]	0.20	0.34	0.52	0.59	0.17	0.31	0.52	0.64	0.23	0.42	0.85	0.80	0.22	0.58	0.87	0.96
ST-Transformer	0.21	0.36	0.58	0.63	0.17	0.30	0.49	0.60	0.22	0.43	0.88	0.82	0.19	0.52	0.79	0.88

milliseconds	Directions				Greeting				Phoning				Posing			
	80	160	320	400	80	160	320	400	80	160	320	400	80	160	320	400
Seq2seq. [24]	0.26	0.47	0.72	0.84	0.75	1.17	1.74	1.83	0.23	0.43	0.69	0.82	0.36	0.71	1.22	1.48
AGED [32]	0.23	0.39	0.63	0.69	0.56	0.81	1.30	1.46	0.19	0.34	0.50	0.68	0.31	0.58	1.12	1.34
DCT-GCN (ST) [23]	0.26	0.45	0.71	0.79	0.36	0.60	0.95	1.13	0.53	1.02	1.35	1.48	0.19	0.44	1.01	1.24
DCT-GCN (LT) [23]	0.29	0.47	0.69	0.76	0.36	0.61	0.97	1.14	0.54	1.03	1.34	1.47	0.21	0.47	1.07	1.31
ST-Transformer	0.25	0.38	0.75	0.86	0.35	0.61	1.10	1.32	0.53	1.04	1.41	1.54	0.61	0.68	1.05	1.28

milliseconds	Purchases				Sitting				Sitting down				Taking photos			
	80	160	320	400	80	160	320	400	80	160	320	400	80	160	320	400
Seq2seq. [24]	0.51	0.97	1.07	1.16	0.41	1.05	1.49	1.63	0.39	0.81	1.40	1.62	0.24	0.51	0.90	1.05
AGED [32]	0.46	0.78	1.01	1.07	0.41	0.76	1.05	1.19	0.33	0.62	0.98	1.10	0.23	0.48	0.81	0.95
DCT-GCN (ST) [23]	0.43	0.65	1.05	1.13	0.29	0.45	0.80	0.97	0.30	0.61	0.90	1.00	0.14	0.34	0.58	0.70
DCT-GCN (LT) [23]	0.50	0.72	1.06	1.12	0.31	0.46	0.79	0.95	0.31	0.64	0.94	1.07	0.17	0.38	0.62	0.74
ST-Transformer	0.43	0.77	1.30	1.37	0.29	0.46	0.84	1.01	0.32	0.66	0.98	1.10	0.15	0.38	0.64	0.75

milliseconds	Waiting				Walking dog				Walking together				Average			
	80	160	320	400	80	160	320	400	80	160	320	400	80	160	320	400
Seq2seq. [24]	0.28	0.53	1.02	1.14	0.56	0.91	1.26	1.40	0.31	0.58	0.87	0.91	0.36	0.67	1.02	1.15
AGED [32]	0.24	0.50	1.02	1.13	0.50	0.81	1.15	1.27	0.23	0.41	0.56	0.62	0.31	0.54	0.85	0.97
DCT-GCN (ST) [23]	0.23	0.50	0.91	1.14	0.46	0.79	1.12	1.29	0.15	0.34	0.52	0.57	0.27	0.52	0.83	0.95
DCT-GCN (LT) [23]	0.25	0.52	0.96	1.17	0.49	0.80	1.11	1.26	0.18	0.39	0.56	0.63	0.30	0.54	0.86	0.97
ST-Transformer	0.22	0.51	0.98	1.22	0.43	0.78	1.15	1.30	0.17	0.37	0.58	0.62	0.30	0.55	0.90	1.02

Table 8: **Long-term H3.6M results** for the four main activities as commonly reported in the literature. Values are the Euler angle metric measured at the given time step (lower is better).

milliseconds	Walking		Eating		Smoking		Discussion		Average	
	560	1000	560	1000	560	1000	560	1000	560	1000
Seq2seq. [24]	0.93	1.03	0.95	1.08	1.25	1.50	1.43	1.69	1.14	1.33
AGED [32]	0.78	0.91	0.86	0.93	1.06	1.21	1.25	1.30	0.99	1.09
DCT-GCN (LT) [23]	0.65	0.67	0.76	1.12	0.87	1.57	1.33	1.70	0.90	1.27
ST-Transformer	0.72	0.78	0.73	1.05	0.89	1.57	1.29	1.85	0.91	1.31